



# Sulfate Adsorption Process from Acid Mine Drainage by Seawater and Acid-Activated Neutralized Red Mud

Mehdi Irannajad<sup>1</sup> · Shima Rahimi<sup>1</sup>

Received: 5 February 2024 / Accepted: 22 April 2024  
© The Tunisian Chemical Society and Springer Nature Switzerland AG 2024

## Abstract

Acid mine drainage (AMD) is an environmental concern which contributed to mining activities and its discharge into surrounding environment can lead to acidification of water bodies and soil. In this research, red mud (RM) with alkaline pH as aluminum industry and alternate adsorbent was studied for the removal of sulfate which can be available in AMD by the batch equilibration technique. Seawater washing and acid treatment were employed as RM modification methods. The results reveal that both methods can decrease high rates of pH and improve the sorption capacity of raw RM. The study also focuses on the effect of various factors on sulfate removal, including acid dosage, pH, adsorbent dose, adsorbate concentration, and contact time. Among these factors, pH is the most important and effective factor in the adsorption of sulfate ions and in strongly acid medium, sulfate adsorption increases due to the high concentration of hydrogen ions and more positive charge on the adsorbent surface. The most sorption capacity and sulfate removal for RM, RMS (RM/Seawater), and RMH (RM/HCl) is equal to 12.7, 15.9 and 23.9 mg/g and 25.5, 31.9 and 41.3% at pH rates of 5.5, 6.5 and 4.5, respectively. Sulfate removal reaches equilibrium in 30, 60 and 60 min contact time for RM, RMS, and RMH, respectively. Based on kinetic studies, pseudo-second order is the best model for sulfate adsorption onto RMS and RMH, and the chemisorption interaction controls step. Isotherm studies demonstrated adsorption is heterogeneous and occurs through particle diffusion and multi-layer and Freundlich model is the best isotherm for description sulfate adsorption on RMH and RMS. FTIR results illustrate a sharp intensity ( $1100\text{ cm}^{-1}$ ) related to  $\text{SO}_4^{2-}$  in RM samples after sulfate adsorption that is sharper for RMH than RMS and RM. EDX studies show increasing Ca peak in RMS due to calcite and aragonite precipitation during seawater treatment and result of acid washing illustrates increasing Fe and Ti peaks in RMH and calcite minerals are decreased. It seems that mononuclear exchange with  $\text{OH}^-$  groups and electrostatic interaction at lower pH, and binuclear ligand exchange with bridge bond formation are the main mechanisms of sulfate adsorption on RM.

**Keywords** Adsorption · Red mud · Sulfate · Isotherm · And kinetic models

## 1 Introduction

Sulfate is generated from the dissolution and chemical or biological oxidation of ores such as pyrite. During the current century, we are witnessing both the declining groundwater level and increased pollution of water resources [1]. Water pollution is a severe global problem that urgently requires concepts for monitoring and implementation plans

deriving solutions [2]. Acid mine drainage (AMD) is well-known as an important source of surface and underground water pollution all over the world. AMD is released when sulfides are exposed to air and water [3]. Also, it often contains elevated levels of sulfate (500–2000 mg/L) and it is produced from electroplating, steel pickling, mining, nonferrous smelting, and other related materials or substances [4]. Sulfates as microscopic particles (aerosols) are generated from dissolution and chemical or biological oxidation ores such as pyrite. They increase the acidity of the atmosphere and form acid rain [5]. The high sulfate content resulted in low-pH water and sulfuric acid formation. This issue is due to the dissolution of toxic and heavy metals and creates unacceptable levels of these metals in water [6]. The production of AMD results in the death of

✉ Mehdi Irannajad  
irannajad@aut.ac.ir

Shima Rahimi  
sh.rahimi1983@gmail.com

<sup>1</sup> Department of Mining Engineering, Amirkabir University of Technology, Tehran, Iran

vegetation and aquatic life, pollution of surface water and groundwater, and corrosion of mine equipment, thus it has become one of the main sources of industrial and environmental pollution [7]. Also, high concentrations of  $SO_4^{2-}$  in aqueous environments can cause the mineralisation of water, corrosion of reinforced steel, scaling of equipment, damage to mammals and endangering human health [8].

Nonetheless, several methods have been employed to treat sulfate-containing wastewater, including chemical precipitation, crystallization [9], ion exchange, biological treatment [10], electro-dialysis [11], nano-filtration [12], adsorption and reverse osmosis [13]. Most processes have significant disadvantages such as a need for high energy and costly process, low efficiency, production of high amounts of sludge, high levels of trace elements, and reclamation processes [6]. Among these processes, adsorption is commonly considered to be the most attractive and most used technique due to its low cost, eco-friendliness, and high performance. An adsorbent can be assumed as low cost if it requires little processing, abundant in nature, or a by-product or waste material from another industry.

Layered double hydroxides (LDH), iron, and aluminum oxides, zeolites, aluminosilicates, activated carbon, graphene, chitin, coir pith, rice straw, and volcanic and fly ash have been applied as adsorbents for sulfate removal from wastewater. High cost and low sorption capacity have always been among the problems of these adsorbents; thus, efforts have continued to find suitable adsorbents in this regard.

Red mud (RM) is produced as an unwanted by-product during the alkaline leaching of bauxite in the Bayer process. According to previous evidence, [14, 15], the production of 1 ton of alumina generally results in the creation of 0.3–2.5 t of RM strongly alkaline ( $pH = 12–13$ ). High alkalinity, large amounts, and fine-grained nature (90% below the size of  $75 \mu m$ ) of RM cause serious environmental problems [16, 17]. It is also composed of a mixture of solid and metallic oxides. The red color arises from iron oxides, which can comprise up to 60% of the mass. The mud is highly basic with a  $pH$  ranging from 10 to 13. In addition to iron, the other dominant components include silica, unleached residual aluminum compounds, and titanium oxide [18, 19]. On the other hand, RM is introduced as an unexpensive adsorbent for various contaminants due to its high metal oxide content and activated compound [14, 20]. Further, various methods of surface modification have been implemented to ameliorate the adsorption properties and enhance the adsorption amount of red mud and its  $pH$  reduction [21]. These methods entail heat activation, acid, and sea water treatment, granular with bentonite or fly ash and presence of different surfactants [22].

According to several reports, RM or activated RM can be utilized for adsorbing different pollutants from water, including phosphate [23, 24], fluoride [25], cadmium, lead,

and copper [26–28], as well as nitrate [29], arsenic [20, 30], phenol [19], methylene blue [22] and dye [31]. Also, RM has been studied as an adsorbent for the removal of ion, polyvalent metal salts and complex species due to its high content of iron and aluminum [32]. However, no study, to the best of our knowledge, has so far focused on using RM for the removal of sulfate from the aqueous phase. Accordingly, the present paper aimed to test RM as an alternate sulfate adsorbent and described the results of an investigation on the sulfate removing characterization of RM.

## 2 Materials and Methods

### 2.1 Materials

RM was provided from the Jajarm mine, which produces RM as an unwanted by-product during the alkaline leaching of bauxite in the Bayer process. This mine is located 5 km from Jajarm in north Khorasan province of Iran. RM was applied as the base material of the adsorbent in this research. Activated RM by seawater and hydrogen chloride (HCl) was used to improve the reactivity of RM as an adsorbent for the removal of sulfate ions in the solution. The sulfate solution was prepared by sodium sulfate ( $Na_2SO_4$ ), and the solution of ionic strength was adjusted using NaCl (1 M). HCl and sodium hydroxide (NaOH) were employed for adjusting the  $pH$  of the solution. Also, reagents were used for sulfate concentration indication in solution by UV–VIS spectrophotometer such as Glycerol and Isopropyl Alcohol. All reagents were supplied from Merck and were illustrated in Table 1.

### 2.2 RM Modification

The following methods were applied to increase the adsorption amount of the adsorbent. Employing RM as adsorbent, it was micronized and then sieved through a 100-mesh screen to obtain  $D_{100}$  of less than  $150 \mu m$ . Next RM was suspended in a solution of seawater with a solid percentage of 10% for 1 h (RMS) and mixed for 1 h to decrease its  $pH$ . This can lead to the precipitation of hydroxide, carbonate or hydroxyl carbonate and a decrease in the  $pH$  rate to 8–8.5. Then, it was filtered and dried in the oven overnight ( $100 \text{ }^\circ\text{C}$ ). Finally, RMS was ground and then sieved through a  $75 \mu m$  screen.

Acid treatment is one of the most important ways of RM modification. In the previous literature, hydrochloric acid has been permanently used as a modifier agent. In the second method, RM was activated using acid treatment with HCl. For the treatment of RM, the RMS was boiled in HCl with different dosages for 1.5 h at the ratio of 1:10 (wt/wt) RM/HCl (RMH) solution. At the end of the experiment, the mixture was centrifuged for 10 min at 3500 r/min. Next, RMH was washed with distilled water and dried overnight at  $100 \text{ }^\circ\text{C}$ .

**Table 1** Used chemical compositions in adsorption experiments

Chemical compound name	Formula	Application	Purity (%)	Company
Distilled water	H <sub>2</sub> O	Adsorption solution	-	Aryateb
Hydrochloric acid	HCl	RM modification	37	Merk
Sodium hydroxide	NaOH	Adjusting pH	95	Merk
Sea water	-	RM modification	-	-
Sodium chloride	NaCl	Adjusting ionic strength	95	Merk
Sodium sulfate	Na <sub>2</sub> SO <sub>4</sub>	Adsorption solution	99	Merk
Glycerol	C <sub>3</sub> H <sub>8</sub> O <sub>3</sub>	Sulfate reagent solution	99	Merk
Isopropyl Alcohol	C <sub>3</sub> H <sub>8</sub> O	Sulfate reagent solution	99	Merk

### 2.3 Batch Adsorption Studies

The adsorption experiments were performed using the batch method in a 250 mL Erlenmeyer flask with a constant stirring rate of 420 rpm, at a temperature of 25 °C, and ionic strength of 0.01 M of NaCl. The sulfate solution with a desired concentration (100–2000 ppm) and contact time (5–120 min) was prepared and placed in contact with raw and activated RM (0.5–5 g L<sup>-1</sup>) and then underwent stirring. Then sulfate solution was prepared with desired concentrations, followed by placing the raw and activated RM in contact with 100 mL sulfate solution and stirring. After equilibrium, the solution was filtered by Whatman filter paper No. 42 and a clear aliquot of the supernatant was taken accordingly. According to previous research, the sulfate percentage in the solution was determined by a UV–VIS spectrophotometer at 420 nm (model HITACHI U-2000) and adding sulfate reagents solution. Ultimately, the sulfate removal (R) and capacity adsorption of the adsorbent (q<sub>e</sub>) were calculated using the Eqs. 1 and 2 [33]:

$$R = \frac{(C_0 - C_e)}{C_0} \times 100 \quad (1)$$

$$q_e = \frac{(C_0 - C_e)}{M} \times V \quad (2)$$

where R is the sulfate removal percentage (%), and C<sub>0</sub> is the initial adsorbate concentration (mg/L). Furthermore, C<sub>e</sub> and q<sub>e</sub> represent the final adsorbate concentration in the solution after equilibrium adsorption (mg/L) and the amount of the adsorbed sulfate per unit of adsorbents (mg/g), respectively. Finally, M is the weight of the adsorbent (g), and V denotes the volume solution (L).

### 2.4 Equilibrium Studies

For equilibrium isotherm investigation, 100 mL of the sulfate solution with various concentrations (250, 500, 750, 1000, 1500, and 2000 ppm) were stirred with 2 g of RMS

and RMH for 60 min at 420 rpm (At this time, used various adsorbents reach the adsorption equilibrium time) at a pH rate of 5.5. The equilibrium isotherms of sulfate adsorption were evaluated by Langmuir, Freundlich, Temkin, and Dubinin Radushkevich models to study the removal amount of sulfate at equilibrium by the unit mass of the adsorbent from the solution at a constant temperature. Equations, Linear expression, and parameters related to these models are presented in Table 2.

For equilibrium isotherm investigation, 100 mL of the sulfate solution with various concentrations (250, 500, 750, 1000, 1500, and 2000 ppm) were stirred with 2 g of RMS and RMH for 60 min at 420 rpm (At this time, used various adsorbents reach the adsorption equilibrium time) at a pH rate of 5.5. The equilibrium isotherms, the solution was filtered by Whatman filter paper No. 42 and a clear aliquot of the supernatant was taken for sulfate percentage measurement in the solution by a UV–VIS spectrophotometer at 420 nm. The equilibrium isotherms of sulfate adsorption were evaluated by Langmuir, Freundlich, Temkin, and Dubinin Radushkevich models to study the removal amount of sulfate at equilibrium by the unit mass of the adsorbent from the solution at a constant temperature. Equations, Linear expression, and parameters related to these models are presented in Table 2 [23].

### 2.5 Kinetic Studies

The adsorption kinetics of sulfate onto RM, RMS, and RMH was evaluated by pseudo-first-order, pseudo-second-order, Elovich, and intraparticle diffusion kinetic models (Table 3) to study the mechanism and rate-controlling step of adsorption [30]. The kinetic model parameters were determined using the least-squares linear regression method. Additionally, the kinetic models of

**Table 2** Isotherm models

Isotherm models	Equations	Linear expression	Parameters
Langmuir	$q_e = \frac{bC_e}{1+bC_e} q_m$	$\frac{C_e}{q_e} = \frac{1}{q_m} b + \frac{C_e}{q_m}$	$q_m$ : (slope) <sup>-1</sup> , b: slope/intercept
Freundlich	$q_e = K_f C_e^{1/n}$	$\log q_e = \log K_f + \frac{1}{n} \log C_e$	$K_f$ : exp(intercept), n: (slope) <sup>-1</sup>
Temkin	$q_e = \frac{RT}{B_T \ln A_T} + \frac{RT}{B_T \ln C_e}$	$q_e = \frac{RT}{B_T \ln A_T} + \frac{RT}{B_T \ln C_e}$	$B_T$ : RT/slope, $A_T$ : exp (intercept $B_T/RT$ )
Dubinin–Radushkevich	$q_e = q_m \exp(-\beta \varepsilon^2)$	$\ln q_e = \ln q_m - \beta \varepsilon^2$	$q_m$ : exp (intercept), $\beta$ : -slope $\varepsilon = RT \ln \left(1 + \frac{1}{C_e}\right)$

the pseudo-first-order and pseudo-second-order were investigated to determine the reaction mechanism (chemical or physical). To examine the kinetic isotherms, the sulfate solution with a concentration of 1000 ppm was stirred by 2 g of the adsorbent at 420 rpm and a pH rate of 5.5 for different times (10, 20, 30, 60, and 120 min), followed by calculating the parameters and validity of the kinetic models (correlation coefficients).

To examine the kinetic isotherms, the sulfate solution with a concentration of 1000 ppm was stirred by 2 g of the adsorbent at 420 rpm and at a pH rate of 5.5 for different times (10, 20, 30, 60, and 120 min), followed by calculating the parameters and validity of the kinetic models (correlation coefficients). The adsorption kinetics of sulfate onto RM, RMS, and RMH was evaluated by pseudo-first-order, pseudo-second-order, Elovich, and intraparticle diffusion kinetic models (Table 3) to study the mechanism and rate-controlling step of adsorption [33]. The kinetic model parameters were determined using the linear regression method of least squares. Additionally, the kinetic models of the pseudo-first-order and pseudo-second-order were investigated to determine the reaction mechanism (chemical or physical).

## 2.6 FTIR Measurement

The FTIR analyses were performed by NEXU670 FT-IR (Nicolet Corporation, USA). The conditioning of suspension was carried out on the adsorbent samples ground under 150  $\mu\text{m}$  similar to the adsorption experiments. In the quantitative analysis, the ratio of KBr to the sample was 300:1 (w/w).

## 2.7 SEM and EDX Studies

Scanning electron microscopy and energy dispersive X-ray (SEM/EDX) spectroscopy (FEI Quanta 200 electron microscopy (Holland)) were applied to determine surface characteristics, morphology and change existing combinations in RM samples.

## 3 Results

### 3.1 XRD and XRF Results

The X-ray fluorescence (XRF) results and X-ray diffraction (XRD) studies of RM are provided in Table 4. XRF results show main chemical compositions in the RM structure are  $\text{Fe}_2\text{O}_3$ ,  $\text{Al}_2\text{O}_3$ ,  $\text{SiO}_2$  and  $\text{CaO}$ . Also, the main minerals in the RM structure are Calcite, Hematite, Diopside, Ilmenite and Sodalite.

### 3.2 Effective Factors on Adsorption

#### 3.2.1 Effect of Acid Dosage

For the activation of raw RM, different dosages of HCl were used, and its effect on sorption capacity and sulfate removal was investigated, the results of which are presented in Table 5. Based on the obtained data, the sorption capacity of the RMH was higher compared to RM. In addition, sulfate adsorption onto RMH increased with the intensification of the acid dosage (in the range of 0.25–1 M). However, the percentage of removal decreased with further enhancements of the acid dosage up to 3 M. Therefore, 1 M was selected as the optimum concentration of HCl.

**Table 3** Kinetic models

Kinetic models	Equations	Linear expression	Parameters
Pseudo-first order	$q_t = q_e [1 - \exp(-k_{1p}t)]$	$\ln(q_e - q_t) = \ln q_e - k_{1p}t$	$q_e = \exp(\text{intercept})$ , $k_{1p} = -(\text{slope})$
Pseudo-second order	$q_t = k_{2p} q_e^2 t / (1 + q_e k_{2p} t)$	$\frac{t}{q_t} = \frac{1}{k_{2p} q_e^2} + t/q_e$	$q_e = \text{slope}^{-1}$ , $k_{2p} = (\text{slope}^2) / \text{intercept}$
Elovich	$q_t = \beta \ln(\beta \alpha t)$	$q_t = \beta \ln(\alpha \beta) + \beta \ln t$	$\beta = \text{slope}$ , $\alpha = (\text{slope})^{-1} \exp(\text{intercept} / \text{slope})$
Intraparticle diffusion	$q_t = k_p t^{0.5}$	$\log q_t = \log k_p + 0.5 \log t$	$k_p = \exp(\text{intercept})$

**Table 4** Chemical and mineralogical compositions of the red mud

Chemical Composition		Mineralogical Composition	
Constituent	% (w/w)	Minerals	Formula
Fe <sub>2</sub> O <sub>3</sub>	22.85	Calcite	Ca <sub>5.23</sub> Mg <sub>0.77</sub> C <sub>6</sub> O <sub>18</sub>
Al <sub>2</sub> O <sub>3</sub>	13.6	Diopside	Ca <sub>3.58</sub> Mg <sub>3.55</sub> K <sub>0.29</sub> Al <sub>0.84</sub> Si <sub>7.74</sub> O <sub>24</sub>
SiO <sub>2</sub>	15.2	Magnetite	Fe <sub>3</sub> O <sub>4</sub>
MgO	1.9	Vermiculite	Si <sub>5.53</sub> Al <sub>3.36</sub> Fe <sub>0.41</sub> Mg <sub>4.04</sub> Ti <sub>0.08</sub> O <sub>30.32</sub> Ca <sub>0.86</sub>
K <sub>2</sub> O	0.53	Ilmenite	FeTiO <sub>3</sub>
TiO <sub>2</sub>	6.9	Katoite	Ca <sub>24</sub> Al <sub>16</sub> Si <sub>24</sub> O <sub>96</sub>
MnO	0.036	hematite	Fe <sub>2</sub> O <sub>3</sub>
CaO	18.8	Rutile	TiO <sub>2</sub>
P <sub>2</sub> O <sub>5</sub>	0.14	Sodalite	Na <sub>2</sub> O.Al <sub>2</sub> O <sub>3</sub> .1.68 SiO <sub>2</sub> .1.73H <sub>2</sub> O
Na <sub>2</sub> O	2.87	Cancrinite	3NaAlSiO <sub>4</sub> .NaOH
SO <sub>3</sub>	0.47		
LOI	16.65		

### 3.2.2 Effect of pH

pH is an important factor in the adsorption of different ions onto the RM surface. The effect of pH on removal percentage and sorption capacity was evaluated using a 2 g/L adsorbent, contact time of 60 min, a sulfate concentration of 1000 ppm and temperature of 27 °C (Fig. 1). The highest sulfate removal and sorption capacity for RM, RMS, and RMH occurred at the pH rates of 5.5, 6.5, and 4.5, that are obtained 25.5, 31.9 and 41.3% and 12.7, 15.9 and 23.9 mg/g, respectively. Considering that a strongly acid medium is due to the high concentration of hydrogen ions and more positive charge on the adsorbent surface, sulfate adsorption increased in these conditions. Furthermore, seawater washing and acid treatment increased sulfate removal and sorption capacity at all pH rates. Moreover, specific adsorption can occur through the ligand exchange mechanism with the displacement of OH<sup>-</sup> groups and sulfates. Therefore, the adsorption of sulfate ions is more intensive under acid conditions [34, 35]. In alkaline conditions, competition between hydroxyl (OH<sup>-</sup>) and sulfate ions with the same negative charge leads to less sulfate adsorption on adsorbent surface. Sulfate adsorption with other natural adsorbents such as

mine waste rocks, minerals, solid waste, clay minerals and soils were increased in acidic pH conditions, and this shows importance of electrostatic interaction and concentration of H<sub>3</sub>O<sup>+</sup> ions in aqueous solution on sulfate adsorption [36].

### 3.2.3 Effect of the Initial Sulfate Concentration

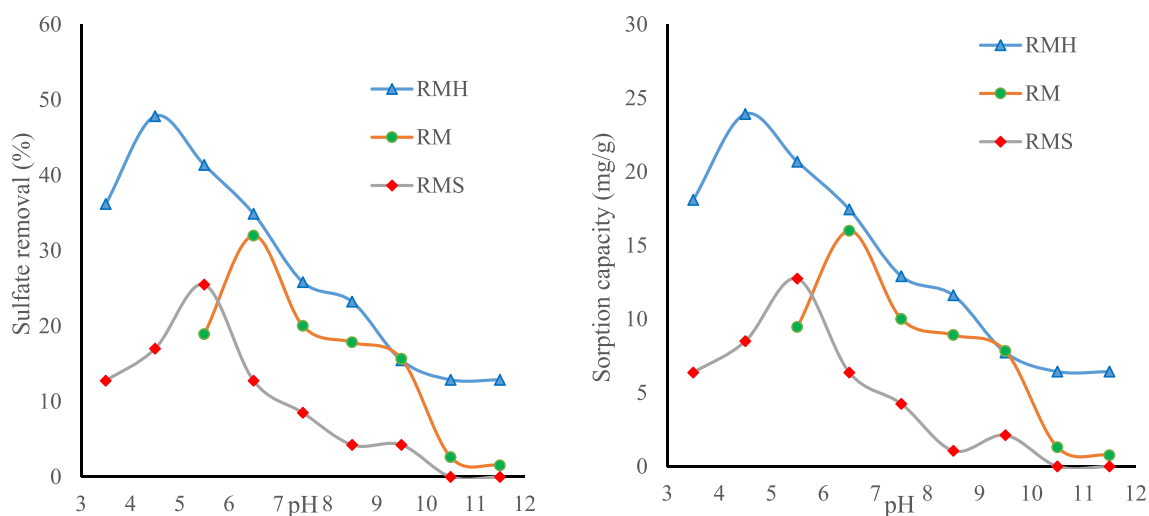
Figure 2 illustrates sulfate adsorption on RM as a function of its initial concentration (100–2000 ppm) at 60 min contact time, optimum pH for each and with a 2 g/L adsorbent. The results indicated that sulfate removal and sorption capacity increase by increasing the sulfate concentration in the solution. It can be concluded that there is no maximum point for the sorption capacity of RMH and RMS, but the sulfate removal percentage reaches an equilibrium state after a 1000 ppm sulfate concentration. The maximum sulfate removal and sorption capacity are gained at 40.4% and 40.4 mg/g for RMH in 2000 ppm sulfate concentration. Similarly, sulfate removal and sorption capacity increase with an increase in the sulfate concentration in the solution, and this is due to the rising of the available sulfate ions in the solution [37]. In the case of other anionic contaminant with same structure as phosphates, with increasing sulfate concentration in the solution; it was increased removal percentage. The most important reason for this can be ligand exchange mechanism, which provide the possibility of increasing the sorption capacity in high concentrations, in the case of anionic ions [38].

### 3.2.4 Effect of Adsorbent Dosage

The effect of RM dosage on sulfate removal from the aqueous solution at the optimum pH is depicted in

**Table 5** The effect of HCl dosage on sulfate removal

Acid Dosage	Sorption Capacity (mg/g)	Sulfate Removal (%)
0.25 M	14.4	28.5
0.5 M	16.5	32.3
1 M	19.2	37.6
2 M	12	24.2
3 M	9.5	18.1



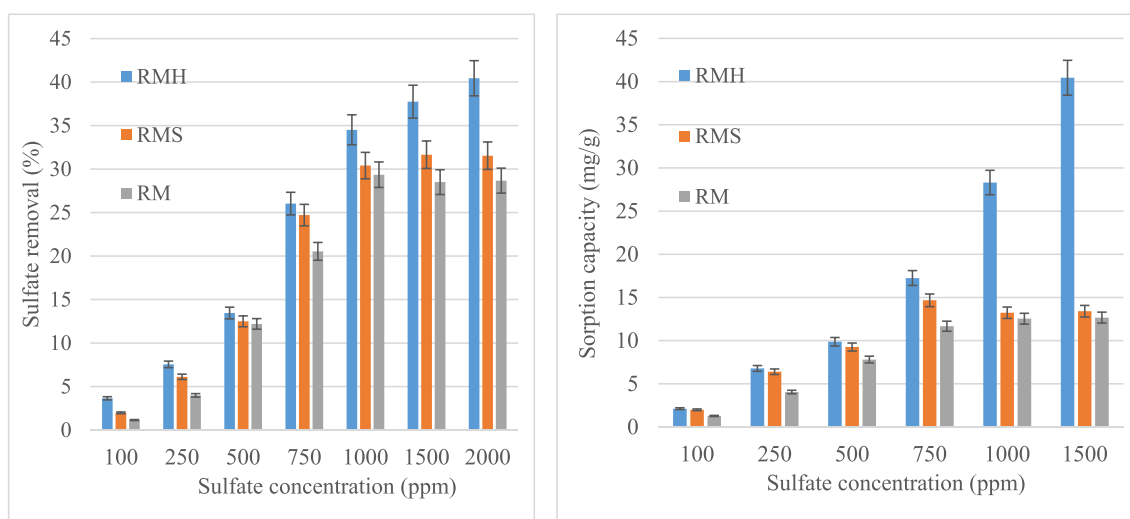
**Fig. 1** Effect of pH on sulfate removal and sorption capacity by RM, RMS, and RMH (adsorbent 2 g/L, contact time of 60 min, sulfate concentration of 1000 ppm and temperature 27 °C)

Fig. 3. As shown, sulfate removal efficiency increases by increasing the RM dosage due to increasing the available surface of the adsorbent. As can be seen, the maximum sulfate removal was 6.3, 29.4 and 33.4% for RM, RMS and RMH in 5 g/L adsorbent dosage. While sorption capacity almost decreases with increasing adsorbent dosage this can be due to a reduction in the number of sulfate ions in the solution compared to adsorbent sites and the maximum sorption capacity are obtained at 38.2, 15.4 and 3.1 mg/g in 0.5, 2 and 4 g/l adsorbent dosage for RMH, RMS and RM, respectively. Further, Fig. 3 confirms that seawater and HCl washing rises sulfate adsorption onto the RM surface. For

other anion contaminants the similar adsorbent dosage of RM is appropriate for adsorption process [39].

### 3.2.5 Effect of the Contact Time

Figure 4 displays the effect of the contact time on the equilibrium of sulfate adsorption onto RM, RMS, and RMH. The sorption capacity increases by increasing time and then remains unchanged in a constant value at a certain time. Based on the results, the adsorption kinetics of sulfate onto RMS and RMH includes two initial rapid reaction steps, and subsequently becomes slow and steady.



**Fig. 2** Effect of the Sulfate concentration on sulfate removal and sorption capacity by RM, RMS, and RMH (adsorbent 2 g/L, contact time of 60 min and temperature of 27 °C)

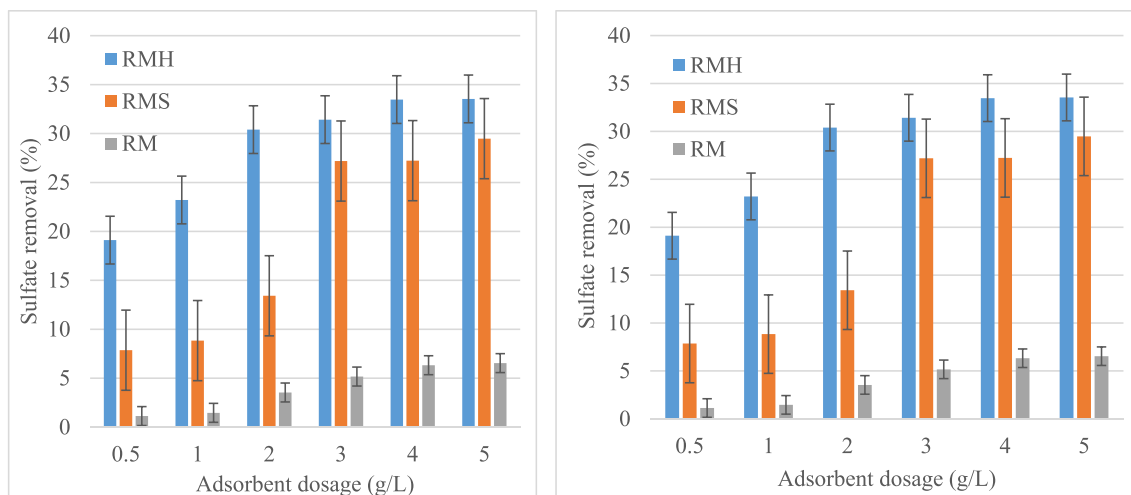


**Fig. 3** Effect of adsorbent dosage on sulfate removal and sorption capacity by RM, RMS, and RMH (contact time of 60 min, sulfate concentration of 1000 ppm and temperature of 27. °C)

The results further demonstrate that the sulfate removal reaches its peak in 30 and 60 min and maximum sulfate removal was 24.7, 29.4 and 33.4% in 120 min contact time for RM, RMS and RMH. A considerable portion of the sulfate adsorption is performed in the initial rapid phase, which can be ascribed to the rapid diffusion of the sulfate ion from the solution to the RMS and RMH external surface [40]. Sorption capacity decreases after reaching the equilibrium time and its maximum is 20.2, 13.5 and 11 mg/g and accrues in 60, 120 and 30 min for RMH, RMS and RM, while removal sulfate percentage increases even after it. It seems that sulfate ions fill all the absorption sites of RM. However, a 60-min period was

considered according to the initial experiments to ensure complete equilibrium. Existence of the initial rapid step in adsorption processes and decreasing adsorption rate in next steps was observed in adsorption of other contaminants on RM surface [41].

### 3.3 Adsorption Isotherm and Kinetic Models

The obtained data from equilibrium tests were modeled using the linear regression method of least squares and correlation coefficient ( $R^2$ ). The isotherm model parameters were determined by the solver add-in function in Microsoft

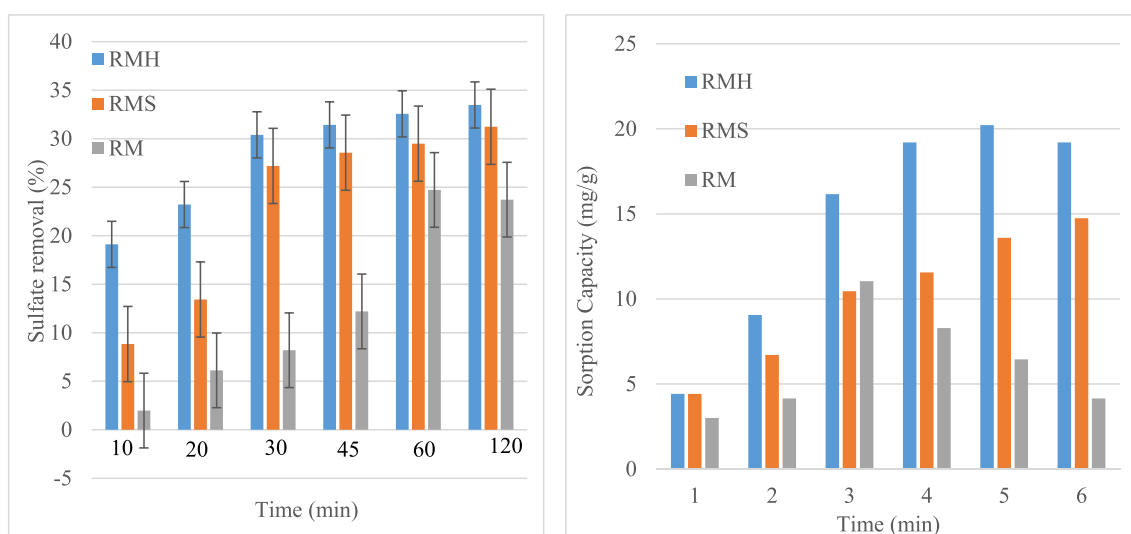


**Fig. 4** Effect of the contact time on sulfate removal and sorption capacity by RM, RMS, and RMH (adsorbent 2 g/L, sulfate concentration of 1000 ppm and temperature of 27. °C)

Excel. Linear expressions, parameters and  $R^2$  related to each model are listed in Table 6.

According to the results of isotherm studies for RMS, the order of the best model based on the  $R^2$  values is Freundlich > Dubinin–Radushkevich > Temkin > Langmuir. For RMH, the matching of the sorption isotherm is almost the same as Bauxsol; the difference is that the matching of Langmuir is more than the Temkin model. There is more matching with the Freundlich model for BRM and RMH with  $R^2$  values 0.97 and 0.94. According to Freundlich isotherm results, maximum sorption capacity for BRM and RMH are obtained at 0.88 and 2.45 mg/g. The Freundlich model indicates that the adsorbent surfaces are heterogeneous and the adsorption onto the adsorbent surface is multilayer. Moreover, adsorption is reversible. In this model, the favorable range of adsorption intensity ( $n$ ) is  $0 < 1/n < 1$ , thus adsorption is desirable down. The Dubinin–Radushkevich model investigates maximum sorption capacity that it indicates 1.37 and 26.3 for BRM and RMH. Also, this model determines the energy of adsorption and type of the adsorption process (physical adsorption ( $E < 8$ ), chemical adsorption or ion exchange ( $E > 16$ ), and particle diffusion that governs the reaction ( $E > 16$ )). Based on this model, the adsorption process occurs with particle diffusion. In this model, it is assumed that the adsorbed amount for any adsorbate concentrations follows a Gaussian function of the Polanyi potential. The Temkin model evaluates the heat of adsorption and some indirect interactions of the adsorbate/adsorbate in the adsorption process. The increase of  $B_T$  for RMH rather than BRM indicates that the acid treatment can improve the adsorption process of sulfate on the RM surface [40–43]. In compared to the other research for investigation of adsorption isotherm of RM, there was the most consistent with the Freundlich isotherm [44].

The adsorption kinetics of sulfate onto RMH and RMH were evaluated by pseudo-first-order, pseudo-second-order, Elovich, and Intraparticle diffusion kinetic models (Table 7) to examine the mechanism and rate-controlling step of adsorption. The  $R^2$  values (0.95 and 0.84 for BRM and RMH) demonstrated that the pseudo-second-order model outperformed the other kinetic models for the description of sulfate adsorption onto both RMH and BRM. These results confirmed that the rate-controlling step in the sulfate adsorption process onto BRM and RMH was a chemisorption interaction. According to this model, two reactions (series or in parallel) are proposed, including the fast reaction that quickly reaches equilibrium and the slow reaction that can continue for a long period [45]. The kinetics constants ( $K$ ) of both pseudo-second-order and intraparticle diffusion models are more for BRM compared to RMH, indicating a further absorption rate of sulfate onto the BRM surface. Contact time for adsorption equilibrium for other applied adsorbents in sulfate adsorption was 60–120 min, so obtained results for kinetic investigation is in good agreement with other results [36].

### 3.4 FTIR Analysis

The FTIR spectra of RM, BRM and RMH after sulfate adsorption on the adsorbent surface in optimum condition are shown in Fig. 5. The bands appearing at 1410–1470  $\text{cm}^{-1}$  for all adsorbents are related to carbonate bands. Also, peak at 1431  $\text{cm}^{-1}$  and 1625  $\text{cm}^{-1}$  for all RM samples corresponds to C–O and C–C stretching vibrations that could be attributed to the existence of cancrinite or calcite in the RM [45, 46]. Furthermore, the bands in the region of 460–590 and 680  $\text{cm}^{-1}$  are the result of the stretching vibrations of the Fe–O bond

**Table 6** Isotherm model parameters for sulfate adsorption onto BRM and RMH

Isotherm Models	Parameters	BRM	RMH
Langmuir	Linear expression	$Y = -1.135X + 755.57$	$Y = -0.4069X + 414.6$
	$q_m$	0.88	2.45
	$b$	-0.001	-0.005
	$R^2$	0.62	0.57
Freundlich	Linear expression	$Y = 2.3411X - 5.6369$	$Y = 2.9026X - 7.1636$
	$K_f$	$2.29 \times 10^{-6}$	$6.68 \times 10^{-8}$
	$N$	2.34	2.9
	$R^2$	0.97	0.94
Temkin	Linear expression	$Y = 5.4182X - 26.981$	$Y = 3.576X - 5.5014$
	$B_T$	468.2	709.4
	$A_T$	0.006	0.21
	$R^2$	0.69	0.32
Dubinin–Radushkevich	Linear expression	$Y = -21.822X + 76.301$	$Y = -0.0378X + 3.27$
	$q_m$	1.37	26.3
	$\beta$	21.8	0.03
	$R^2$	0.84	0.84



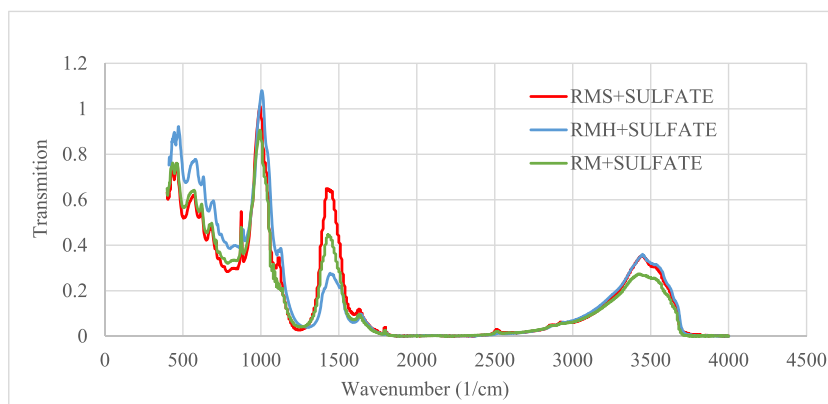
**Table 7** Kinetic model parameters for sulfate adsorption onto BRM and RMH

Isotherm Models	Parameters	BRM	RMH
Pseudo-first-order	Linear expression	$Y = 0.0087X + 1.8443$	$Y = 0.0106X + 2.046$
	$q_e$	6.32	7.73
	$K_1$	0.008	0.01
	$R^2$	0.51	0.42
Pseudo-second-order	Linear expression	$Y = 0.0545X + 1.3812$	$Y = 0.0377X + 1.2337$
	$q_e$	18.34	26.52
	$K_2$	0.19	0.17
	$R^2$	0.95	0.84
Elovich	Linear expression	$Y = 4.3641X - 4.3701$	$Y = 6.8858X - 9.9079$
	$\alpha$	0.33	0.23
	$\beta$	0.22	0.14
	$R^2$	0.79	0.81
Intraparticle diffusion	Linear expression	$Y = 1.6056X$	$Y = 0.2365X$
	$K_p$	1.6	0.23
	$R^2$	0.62	0.63

that can be associated with hematite and magnetite as the main composition of red mud. Additionally, the bands at around  $995\text{ cm}^{-1}$  may correspond to the Si–O–Si and Si–O–Al vibrations that could belong to alumina, Zhypst and Boehmite in RM [23, 19]. The peak intensity of calcite ( $1431\text{ cm}^{-1}$ ) in BRM spectra becomes sharper rather than other adsorbents and the peak related to OH ( $3420\text{ cm}^{-1}$ ) is reduced due to the neutralized OH ion with Mg, Al and Ca in seawater. In the case of RMH, the CaO band  $874\text{ cm}^{-1}$  disappears due to its reaction with HCl and the dissolution of calcite and cancrinite [23]. In addition, Al–O and Fe–O bands ( $460\text{--}590$  and  $680\text{ cm}^{-1}$ ) in the RMH spectrum have become weaker due to the possible dissolution of Fe and Al oxides/hydroxides [46]. As can be seen, there is a sharp intensity absorption around  $1100\text{ cm}^{-1}$  that is related to the  $\text{SO}_4^{2-}$  vibration band in RM, BRM and RMH after sulfate adsorption. The intensity of this peak is sharper for RMH than BRM and RM, this issue shows more adsorption of sulfate on RMH.

### 3.5 SEM and EDX Results

Scanning electron microscopic pictures related to RM, RMS and RMH are shown in Fig. 6 in a, b and c sections, respectively. There are particles of various sizes and amorphous or crystalline structures. Metal oxide and primitive minerals especially iron have crystalline structures and large sizes and amorph minerals that were formed during the Bayer process including sodium and aluminum minerals are smaller. EDX results in Fig. 7 illustrate the attendance of iron, calcium, titanium and silicon as main constituent elements in RM, RMS and RMH structures. Comparing the EDX result of RMS with RM shows increasing calcium ions in RMS composition due to calcite and aragonite precipitation during seawater treatment. In the RMH sample, peaks related to iron and titanium ions are increased meanwhile, calcite minerals are decreased as result of acid washing.

**Fig. 5** FTIR of red mud samples after sulfate adsorption

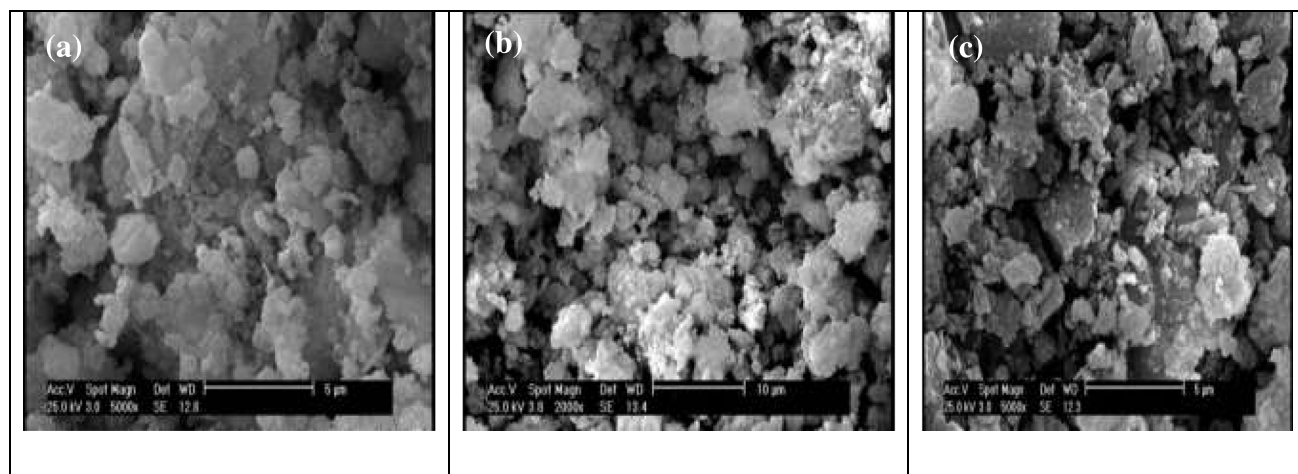


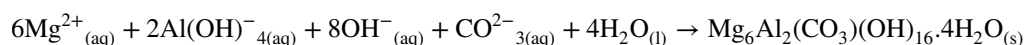
**Fig. 6** Scanning electron microscopic of RM (a) RMS (b) and RMH (c)

## 4 Discussion

According to surveys, modifications with seawater and hydrochloric acid can improve the absorption properties of RM as the adsorbent of the sulfate ion from the aqueous solution. The XRF results of RM, RMS, and RMH are summarized in Table 8. Chemical compounds related to calcium and magnesium increased in RMS compared to RM. The seawater treatment can lead to the sediment of calcium, magnesium,

and aluminum ions as hydroxide, carbonate, and bicarbonate on the RM surface. On the other hand, seawater washed and decreased sodium ions from the RM surface, leading to a decline in the alkalinity of raw RM, while an increase in capacity adsorption. In addition, seawater addition and presence of  $Mg^{2+}$  led to the formation of Mg/Al LDH phases (e.g., hydroxalite  $(Mg_6Al_2(CO_3)(OH)_{16} \cdot 4H_2O)$  as Eq. (1) and carbonate precipitation. LDH minerals contain an interlayer site occupied by anions, usually carbonate or sulfate [47].

(3)



The chemical composition of RMH indicated that sodium and calcium ions decrease with acid treatment, leading to an increase in the specific surface of RMH in comparison to RM [48]. On the other hand, metal compounds in RMH (e.g., aluminum and titanium) decrease, but the amount of iron

compounds remains constant, implying that hydrochloric acid with a 1 M concentration is incapable of the dissolution of iron ions. The acid treatment creates appropriate functional groups and increases positive charge ( $H^+$  ions) onto the RM surface for the adsorption of sulfate anions [48]. Using concentrated

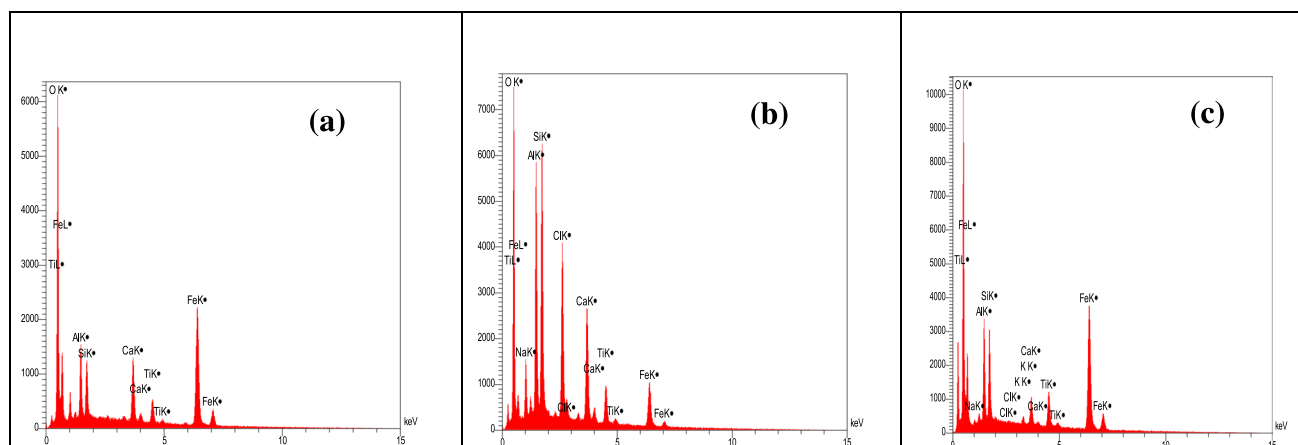


**Fig. 7** Energy dispersive X-ray of RM (a) RMS (b) and RMH (c)

**Table 8** Chemical compounds basis on XRF for RM, RMS, and RMH

Compounds	Fe <sub>2</sub> O <sub>3</sub>	Al <sub>2</sub> O <sub>3</sub>	SiO <sub>2</sub>	MgO	K <sub>2</sub> O	TiO <sub>2</sub>	MnO	CaO	P <sub>2</sub> O <sub>5</sub>	Na <sub>2</sub> O	Cl	LOI
RM	22.7	12.1	15.4	1.2	0.83	6.8	0.1	18.1	0.15	2.83	0.37	
RMS	22.5	13.3	15.2	1.7	0.53	6.7	0.104	18.5	0.14	2.57	0.47	16.6
RMH	22.2	15.1	17.3	1.82	0.4	7.1	0.105	17.4	0.14	2.39	0.67	14.4

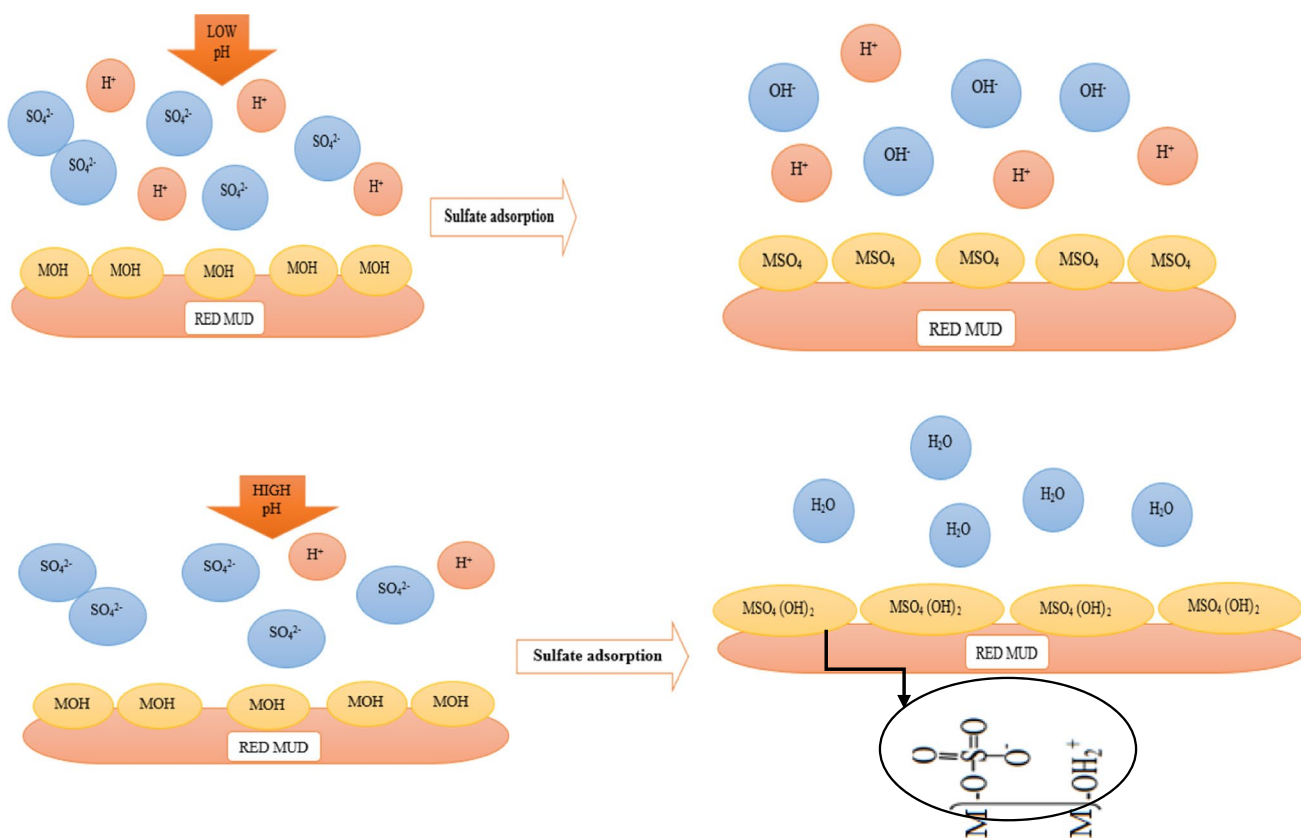
acid can remove iron and aluminum oxide groups and decrease the adsorption of sulfate ions by RMH [23]. Likewise, acid treatment reduces organic and non-organic impurities in RM and forms micro and macro pores on the RM surface.

The initial sulfate concentration in the solution is an effective factor in the mechanism of sulfate adsorption. At low concentrations of sulfate, groups (Al-OH<sub>2</sub> or Fe-OH<sub>2</sub>) are formed from the positive sites on the adsorbent surface. The proportions of sulfate to hydroxyl groups increase (Al-OH) from the neutral sites by an increase in the concentration [48]. In the case of adsorbent dosage, its increase may lead to the overlap of activated adsorption sites and sequent reduction in the capacity adsorption of the adsorbent [49]. Totally, the adsorption time of sulfate is short. Sulfate adsorption onto BRM and RMH becomes slow and gradual after rapid initial adsorption [50].

In a strongly acid medium, sulfate adsorption increases due to the high concentration of hydrogen ions and more positive charge on the adsorbent surface [51]. Specific

adsorption can occur through the ligand exchange mechanism, the displacement of OH<sup>-</sup> groups by sulfates. Therefore, the adsorption of sulfate ions is more intensive under acid conditions [23]. In alkaline conditions, competition between hydroxyl (OH<sup>-</sup>) and sulfate ions with the same negative charge causes less sulfate adsorption on adsorption. Accordingly, there are two mechanisms of adsorption as follows:

1. Mononuclear ligand exchange with OH<sup>-</sup> groups and possible electrostatic interaction are observed at lower pH rates.
2. At high pH rates, the binuclear ligand exchange is detected with the formation of a bridge bond [50]. Additionally, it is supposed that sulfates can be adsorbed by Al hydroxides with binuclear bridging over mononuclear exchange [49]. Figure 8 shows schematic sulfate adsorption at low and high pH rates onto RM.

**Fig. 8** Sulfate adsorption at low and high pH rates onto the red mud

Based on the results of isotherm studies, row and activated RM surfaces are heterogeneous, and the adsorption process is multilayer. Further, sulfate adsorption onto RMS and RMH occurs through particle diffusion, which has the property of reversibility [23]. More matching of kinetic data with the pseudo-second-order model indicates that the adsorption process is of chemical type, and the initial sulfate concentration and the number of activated sites adsorbents in the solution are both effective factors in adsorption [51].

## 5 Conclusion

- Both seawater and acid treatment methods can modify high pH of red mud and improve its sorption capacity.
- The maximum sorption capacity and sulfate removal for RM, RMS, and RMH are obtained 12.7, 15.9 and 23.9 mg/g and 25.5, 31.9 and 41.3% in pH equal to 5.5, 6.5 and 4.5.
- Sulfate adsorption on RMH, RMS and RM reaches to equilibrium time after 60, 30 and 30 min and the maximum sorption capacity is 20.2, 13.5 and 11 mg/g, respectively.
- According to isotherm studies, the most matching is the Freundlich model for RMS and RMH and maximum sorption capacity is obtained at 0.88 and 2.45 mg/g.
- Isotherm studies demonstrated RM surface is heterogeneous and adsorption occurs through particle diffusion and multilayer.
- $B_T$  parameter in the Temkin model indicates that acid treatment can improve the adsorption process of sulfate on the RM surface better than seawater and it is consistent with the obtained results.
- Pseudo-second-order is the best kinetic model for the description of sulfate adsorption onto RMH and BRM and confirms rate-controlling step is a chemisorption interaction.
- FTIR results showed that there is a sharp intensity in  $1100\text{ cm}^{-1}$  that is related to the  $\text{SO}_4^{2-}$  vibration band in RM samples after sulfate adsorption and its peak is sharper for RMH than BRM and RM.
- Mononuclear ligand exchange with  $\text{OH}^-$  groups and electrostatic interaction at lower pH and binuclear ligand exchange at high pH rates can be as adsorption mechanisms of sulfate on RMH.

## References

1. Singh J, Yadav P, Pal AK, Mishra V (2020) Water Pollutants: Origin and Status. In: Pooja D, Kumar P, Singh P, Patil S (eds) *Sensors in Water Pollutants Monitoring: Role of Material. Advanced Functional Materials and Sensors*. Springer, Singapore, pp 5–20
2. Manisalidis, I., Stavropoulou, E., Stavropoulos, A., Bezirtzoglou, E.: Environmental and Health Impacts of Air Pollution: A Review. *Front Public Health* 8 (2020)
3. Alimohammadi V, Sedighi M, Jabbari E (2017) Optimization of sulfate removal from wastewater using magnetic multi-walled carbon nanotubes by response surface methodology. *Water Sci Technol* 76(10):2593–2602
4. Kitadai N, Nishiuchi K, Tanaka M (2018) A comprehensive predictive model for sulfate adsorption on oxide minerals. *Geochim Cosmochim Acta* 238(1):150–168
5. Fanning, D.S., Rabenhorst, M.C., Burch, S.N., Islam, K.R., Tangren, S.A.: *Soil mineralogy with environmental applications, Chapter 7: Sulfides and sulfates*. (2002)
6. Halajnia A, Oustan S, Najafi N, Khataee AR, Lakzian A (2013) Adsorption–desorption characteristics of nitrate, phosphate and sulfate on Mg–Al layered double hydroxide. *Appl Clay Sci* 80(1):305–312
7. Baldwin DS, Mitchell A (2012) Impact of sulfate pollution on anaerobic biogeochemical cycles in a wetland sediment. *Water Res* 46(4):965–974
8. Runtti H, Luukkonen T, Niskanen M, Tuomikoski S, Kangas T, Tynjala P, Tolonen E-T, Sarkkinen M, Kempainen K, Ramo J, Lassi U (2016) Sulphate removal over barium-modified blast-furnace-slag geopolymer. *J Hazard Mater* 317:373–384
9. Silva AM, Lima MF, Leão A (2012) Mine water treatment with limestone for sulfate removal. *J Hazard Mater* 221(1):45–55
10. Liang F, Xiao Y, Zhao F (2013) Effect of pH on sulfate removal from wastewater using a bioelectrochemical system. *Chem Eng J* 218(1):147–153
11. Lee HJ, Oh SJ, Moon SH (2003) Recovery of ammonium sulfate from fermentation waste by electrodialysis. *Water Res* 37(5):1091–1099
12. Galiana-Aleixandre MV, Iborra-Clar A, Bes-Pifi A, Mendoza-Roca JA, Cuartas-Urbe B, IborraClar MI (2005) Nanofiltration for sulfate removal and water reuse of the pickling and tanning processes in a tannery. *Desalination* 179(1–3):307–313
13. Bodalo A, Gomez JL, Gomez E, Leon G, Tejera M (2004) Reduction of sulphate content in aqueous solutions by reverse osmosis using cellulose acetate membranes. *Desalination* 162(10):55–60
14. He J, Jie Y, Zhang J, Yu Y, Zhang G (2013) Synthesis and characterization of red mud and rice husk ash-based geopolymer composites. *Cement Concr Compos* 37:108–118
15. Liu Y, Naidu R, Ming H (2011) Red mud as an amendment for pollutants in solid and liquid phases. *Geoderma* 163(1–2):1–12
16. Zhao Y, Yue Q, Li Q, Xu X, Yang Z, Wang X, Gao B, Yu H (2012) Characterization of red mud granular adsorbent (RMGA) and its performance on phosphate removal from aqueous solution. *Chem Eng J* 193:161–168
17. Ye J, Cong X, Zhang P, Hoffmann E, Zeng G, Liu Y, Fang W, Wu Y, Zhang H (2015) Interaction between phosphate and acid-activated neutralized red mud during adsorption process. *Appl Surf Sci* 356:128–134
18. Sutar H, Mishra SCh, Sahoo S, Chakraverty AP (2014) Progress of red mud utilization: an overview. *Am Chem Sci J* 4(3):255–279
19. Burke IT, Peacock CL, Lockwood CL, Stewart DI, Mortimer RJG, Ward MB, Renforth P, Gruiz K, Mayes WM (2013) Behavior of aluminum, arsenic, and vanadium during the neutralization of red mud leachate by HCl, gypsum, or seawater. *Environ Sci Technol* 47(12):6527–6535
20. Palmer SJ, Nothling M, Bakon KH, Frost RL (2010) Thermally activated seawater neutralized red mud used for the removal of arsenate, vanadate and molybdate from aqueous solutions. *J Colloid Interface Sci* 342(1):147–154
21. Schwarz, S., Schwarz, D., Ohmann, W., Neuber, S.: Adsorption and desorption studies on reusing chitosan as an efficient adsorbent. *Proceedings of the 3rd World Congress on Civil, Structural and Environmental Engineering*, 8 – 10 (2018)
22. Martins YJC, Almeida ACM, Viegas BM, Nascimento RA, Ribeiro NF (2020) Use of red mud from amazon region as an adsorbent for the removal of methylene blue: process optimization, isotherm and kinetic studies. *Int J Environ Sci Technol* 17:4133–4148

23. Ye J, Cong X, Zhang P, Zeng G, Hoffmann E, Wu Y, Zhang H, Fang W (2016) Operational parameter impact and back propagation artificial neural network modeling for phosphate adsorption onto acid-activated neutralized red mud. *J Mol Liq* 216:35–41
24. Somogyi V, Pitas V, Berta KM, Kurdi R (2022) Red mud as adsorbent to recover phosphorous from wastewater streams. *Sustainability* 14:1–15
25. Smičiklas I et al (2013) The influence of citrate anion on Ni (II) removal by raw red mud from aluminum industry. *Chem Eng J* 214(2):327–335
26. Li D, Ding Y, Li L, Chang Z, Rao Z, Lu L (2015) Removal of hexavalent chromium by using red mud activated with cetyltrimethylammonium bromide. *Environ Technol* 36(9):1084–1090
27. Sahu M, Mandal S, Dash S, Badhai P, Patel R (2013) Removal of Pb (II) from aqueous solution by acid activated red mud. *J Environ Chem Eng* 1(4):1315–1324
28. Zhang DR, Chen H, Xia J, Nie Z, Zhao X, Pakostova E (2023) Novel adsorbent synthesized from red mud and acid mine drainage for enhanced contaminant removal: industrial waste transformation, adsorbent performance and metal(loid) removal mechanisms. *Chem Eng J* 465(1):142867
29. Gupta V, Gupta M, Sharma S (2010) Process development for the removal of lead and chromium from aqueous solutions using red mud an aluminium industry waste. *Water Res* 35(5):1125–1134
30. Apak R, Tutem E, Ugul MH, Hizal J (1997) Heavy metal cation retention by unconventional sorbents (red muds and fly ashes). *Water Res* 32(2):430–440
31. Tor A, Cengeloglu Y, Aydin ME, Ersoz M (2006) Removal of phenol from aqueous phase by using neutralized red mud. *J Colloid Interface Sci* 300(2):498–503
32. Chmielewski E, Sabova L, Peterlik H, Wu A (2011) Batch-wise adsorption, xaxs and microscopic studies of zeolite pelletized with biopolymeric alginate. *Braz J Chem Eng* 28(1):63–71
33. Deihimi N, Irannajad M, Rezai B (2018) Equilibrium and kinetic studies of ferricyanide adsorption from aqueous solution by activated red mud. *J Environ Manage* 227(1):277–285
34. Sokolova TA, Alekseeva SA (2008) Adsorption of sulfate ions by soils (A review). *Eurasian Soil Sci* 41(2):140–148
35. Dolatabadi, A.A., Ganjidoust, H., Ayati, B.: Application of waste-derived activated red mud/base treated rice husk composite in sulfate adsorption from aqueous solution. *Int J Environ Res* 16(2) (2022)
36. Sadeghalvad B, Khorshidi N, Azadmehr A, Sillanpa M (2011) Sorption, mechanism, and behavior of sulfate on various adsorbents: a critical review. *Chemosphere* 263:128064
37. Sadeghalvad B, Azadmehr A, Hezarkhani A (2016) Enhancing adsorptive removal of sulfate by metal layered double hydroxide functionalized quartz albitophire iron ore. *RSC Adv* 72:1–13
38. Zhao Y, Wang J, Luan Z, Peng X, Liang Z, Shi L (2009) Removal of phosphate from aqueous solution by red mud using a factorial design. *J Hazard Mater* 165(1–3):1193–1199
39. Deihimi N, Irannajad M, Rezai B (2018) Prediction of removal percentage and adsorption capacity of activated red mud for removal of cyanide by artificial neural network. *Geosyst Eng* 21(5):1–9
40. Gimbert F, Morin-Crini N, Renault F, Badot PM, Crini G (2008) Adsorption isotherm models for dye removal by cationized starch-based material in a single component system: error analysis. *J Hazard Mater* 157(1):34–46
41. Cengeloglu Y, Tor A, Ersoz M, Arslan G (2006) Removal of nitrate from aqueous solution by using red mud. *Sep Purif Technol* 51(3):374–378
42. Castaldi P, Silveti M, Garau G, Deiana S (2010) Influence of the pH on the accumulation of phosphate by red mud (a bauxite ore processing waste). *J Hazard Mater* 182(1–3):266–272
43. Li D, Ding Y, Li L, Chang Z, Rao Z, Lu L (2015) Removal of hexavalent chromium by using red mud activated with cetyltrimethylammonium bromide. *Environ Technol* 36(9–12):1084–1090
44. Deihimi N, Irannajad M, Rezai B (2019) Removal of ferricyanide ions from aqueous solutions using modified red mud with cetyl trimethylammonium bromide. *Environ Earth Sci* 78(6):187
45. Deihimi N, Irannajad M, Rezai B (2018) Characterization studies of red mud modification processes as adsorbent for enhancing ferricyanide removal. *J Environ Manage* 206(1):266–275
46. Prakash S, Das B, Mohanty JK, Venugopal R (1999) The recovery of fine mineral from quartz and corundum mixtures using selective magnetic coating. *Int J Miner Process* 57(5):87–103
47. Ye J, Cong X, Zhang P, Hoffmann E, Zeng G, Liu Y, Fang W, Wu Y, Zhang H (2015) Interaction between phosphate and acid-activated neutralized red mud during adsorption process. *Appl Surf Sci* 356(1):128–134
48. Wang X, Wang Z, Peak D, Tang Y, Feng X, Zhu M (2018) Quantification of coexisting inner-and outer-sphere complexation of sulfate on hematite surfaces. *ACS Earth Space Chem* 2(4):387–398
49. Tor A, Danaoglu N, Arslan G, Cengeloglu Y (2009) Removal of fluoride from water by using granular red mud: batch and column studies. *J Hazard Mater* 164(1):271–278
50. Kitadai N, Nishiuchi K, Tanaka M (2018) A comprehensive predictive model for sulfate adsorption on oxide minerals. *Geochim Cosmochim Acta* 238:150–168
51. Zhu M, Northrup P, ShiSimon Ch, Billinge JL, Sparks DL, Waychunas GA (2014) Structure of sulfate adsorption complexes on ferrihydrite. *Environ Sci Technol Lett* 1(1):97–101

Springer Nature or its licensor (e.g. a society or other partner) holds exclusive rights to this article under a publishing agreement with the author(s) or other rightsholder(s); author self-archiving of the accepted manuscript version of this article is solely governed by the terms of such publishing agreement and applicable law.